Nonlinear dynamics of multiple four-wave mixing processes in a single-mode fiber

John R. Thompson and Rajarshi Roy
School of Physics, Georgia Institute of Technology, Atlanta, Georgia 30332
(Received 15 November 1990)

Multiple four-wave mixing processes in an optical fiber are investigated both theoretically and experimentally. The propagation equations for the complex amplitudes of two pump waves (angular frequencies ω_1 and ω_2) and four sidebands ($\omega_3=2\omega_1-\omega_2$, $\omega_4=2\omega_2-\omega_1$, $\omega_5=2\omega_3-\omega_1$, and $\omega_6=2\omega_4-\omega_2$) are derived. These six waves interact through seven partially degenerate and nondegenerate four-wave mixing processes. Conservation relations for the wave amplitudes are obtained. Numerical integration of these equations reveals both periodic and chaotic energy exchange between the pump waves and sidebands. Predictions from the model are tested directly by experimental measurements on a single-mode optical fiber.

I. INTRODUCTION

The study of nonlinear optical interactions of multiple waves propagating through an optical fiber is of immediate concern for considerations of wavelength multiplexing in optical communications. Four-wave mixing (FWM) processes are highly relevant in this context, particularly for short fiber lengths, in which Raman generation is not a dominant process.[1] In the past, four-wave mixing in optical fibers has been investigated by several authors;[1-6] these investigations have been motivated mostly by the production of new frequency sources or by the parametric amplification of signals. Optical fibers are an ideal medium for the study of nonlinear dynamical effects in wave propagation because of the low losses and high power densities that are easily achieved in single-mode fibers.[7] These studies generally concerned themselves with a single degenerate or nondegenerate FWM process. Analytic solutions have been obtained for such cases, even when the depletion of the pump waves is accounted for. Hamiltonian chaos in the polarization dynamics of birefringent fibers has also been studied by several authors.[8,9]

Situations where multiple nonlinear interactions between several waves may occur are more complex, and such systems are often nonintegrable and display chaotic dynamics. As an example of such a system, Alekseev *et al.*[10,11] have theoretically studied instabilities in a nonlinear optical medium with six propagating light waves all at the same frequency but with different wave vectors. They have predicted the occurrence of chaotic energy exchange between the waves under certain conditions and for certain regimes of parameters.

In this paper, we consider an experimentally realizable system that is closely related to the ones described by Alekseev *et al.*; six waves of the same linear polarization, but with different frequencies, propagate in an optical fiber and interact through the third-order Kerr nonlinearity of the medium. For short propagation lengths, optical fibers provide an essentially lossless system that can display periodic and chaotic energy transfer between multiple propagating waves. Several competing FWM processes may occur in the fiber that are, in general, not phase matched. In our experiments, two pump waves detuned from each other (with angular frequencies ω_1 and ω_2) generate two "first-order" sidebands at $\omega_3=2\omega_1-\omega_2$ and $\omega_4=2\omega_2-\omega_1$. If the first-order sidebands grow sufficiently strong through energy depletion of the pump waves, they may then interact with the pump waves to generate "second-order" sidebands at $\omega_5=2\omega_3-\omega_1$ and $\omega_6=2\omega_4-\omega_2$. The system of equations that describes these six propagating waves displays a rich variety of nonlinear dynamical behavior, and it is possible to test the predictions of this model experimentally. We limit ourselves to wave intensities such that the second-order sidebands never contain more than a few percent of the pump energy.

In Sec. II, we derive the propagation equations for the complex amplitudes of the six waves in the nonlinear medium. The conditions for which our model is valid and the approximations necessary for the derivation are discussed. Energy conservation is shown to follow from these equations for the lossless fiber, and a second conserved quantity for the system of equations is obtained. We describe the results obtained from numerical integration of the propagation equations in Sec. III. Periodic and chaotic energy exchange between the pump waves and sidebands is observed and investigated as a function of pump energy and detuning between the pump waves. Section IV presents experimental evidence of the validity of the theoretical model. Direct tests of predictions obtained from the propagation equations are described. It is shown that it is necessary to include the second-order sidebands to obtain good agreement between experiment and theory.

II. COMPLEX AMPLITUDE PROPAGATION EQUATIONS

The nonlinear propagation equations for the complex amplitudes of the six frequency components interacting via self-phase-modulation (SPM), cross-phase modulation

(XPM), and FWM can be derived from Maxwell's equations by including the appropriate terms of the nonlinear polarization of the fiber medium. Before proceeding in detail, the conditions and simplifying assumptions for our derivation will be outlined. We assume that the fields are linearly polarized so that a scalar approach can be taken. Also, the fiber is assumed to support only a single transverse mode. The transverse modes are assumed to remain essentially undisturbed by the perturbing nonlinearity. Absorption loss and Raman scattering are neglected in this model. We take the quasi-cw approximation neglecting dispersion and walkoff of the different frequency components since the fiber lengths used in experiments and numerical calculations are much shorter than the characteristic dispersion and walkoff lengths for our pulse widths (~ 5 ns).[4] Finally, the frequencies of the six waves are assumed to be relatively close so that differences in material refractive index and frequency are very small.

We first consider the linear propagation of pulses through an optical fiber. We will derive the equation for the transverse modes and utilize this later to simplify the nonlinear wave equations. Assuming no free charges or currents and no induced magnetization, the wave equation, in terms of the electric field and induced polarization, will take the form

$$\nabla^2 E - \mu_0 \epsilon_0 \frac{\partial^2 E}{\partial t^2} = \mu_0 \frac{\partial^2 P}{\partial t^2} \ . \tag{1}$$

Now the linear polarization can be related to the electric field by the constitutive relationship $P = \epsilon_0 \chi^{(1)} E$. Since we are neglecting the absorption losses we can ignore the imaginary part of the susceptibility $\chi^{(1)}$ and the material refractive index will be given by $n_0 = (1+\chi^{(1)})^{1/2}$. Using these facts the wave equation becomes

$$\nabla^2 E - \frac{n_0^2}{c^2} \frac{\partial^2 E}{\partial t^2} = 0 \ . \tag{2}$$

For simplicity we will consider a plane-wave solution expressed as the product of functions of the transverse coordinates r and ϕ and the axial coordinate z,

$$E = \psi(r,\phi) \exp[i(\beta z - \omega t)] + \text{c.c.} \ , \tag{3}$$

where c.c. denotes the complex conjugate. The quantity β is the axial propagation constant that is dependent on the transverse mode in which the wave propagates. The only time and z dependence we are considering is contained in the oscillatory plane-wave part of the field. Substituting Eq. (3) in Eq. (2), the time derivatives and the axial part of the Laplacian can be immediately simplified to yield the following equation for the transverse part of the electric field

$$\nabla_T^2 \psi + (k_0^2 - \beta^2)\psi = 0 \ . \tag{4}$$

Here, $k_0 = n_0 \omega / c$, with only the material index taken into account while β takes into account both material and waveguiding effects. The quantity ∇_T^2 denotes the transverse part of the Laplacian. The solution to this equation gives the transverse modes in the fiber. These will be products of Bessel functions in the radial coordinate and trigonometric functions for the azimuthal angle.[4,12] The exact form of these solutions is not of concern here. Now let us consider the nonlinear propagation of several frequency components.

In general the solutions to our wave equations will not be monochromatic plane waves, and the material polarization will not be simply a linear function of the electric field. In this derivation of the equations governing the propagation of the different frequency components we will assume each wave to be monochromatic, but the slowly varying envelopes will depend on z. This alone will not greatly complicate the solution; we can still separate variables and get an equation identical to Eq. (4) for the transverse modes of the fiber. The difficulty is caused by the nonlinear polarization which will prevent a separation of variables. This is overcome by treating the nonlinearity as a small perturbation and assuming that the transverse modes are essentially unperturbed by the nonlinearity. This will allow us to get propagation equations for the z-dependent part of the wave amplitudes and integrate out the transverse coordinates leaving a constant related to the mode size.[1,4] The starting point is the wave equation for the electric field and polarization. Now we will include a cubic term in the polarization so that

$$P = \epsilon_0 (\chi^{(1)} E + \chi^{(3)} E^3) \ . \tag{5}$$

From the relationship for the material refractive index, $n_0 = (1+\chi^{(1)})^{1/2}$, one gets the nonlinear wave equation to be

$$\nabla^2 E - \frac{n_0^2}{c^2} \frac{\partial^2 E}{\partial t^2} = \frac{\chi^{(3)}}{c^2} \frac{\partial^2 E^3}{\partial t^2} \ . \tag{6}$$

To proceed further we must write the electric field in terms of its frequency components. For the FWM processes of interest there will be six frequencies: two pump frequencies at ω_1 and ω_2, two first-order sidebands at $\omega_3 = 2\omega_1 - \omega_2$ and $\omega_4 = 2\omega_2 - \omega_1$, and two second-order sidebands at $\omega_5 = 2\omega_3 - \omega_1$ and $\omega_6 = 2\omega_4 - \omega_2$. Thus the electric field can be written as

$$E = \tfrac{1}{2} \sum_{m=1}^{6} \{ E_m(\mathbf{r}) \exp[i(\beta_m z - \omega_m t)] + \text{c.c.} \} \ , \tag{7}$$

where $\beta_m = n_m \omega_m / c$ is the axial propagation constant and includes material and waveguiding effects in the refractive index. Following the treatment of Stolen and Bjorkholm,[1] it will be convenient to express the field amplitudes in a form easily related to the power in the wave. First, separate the field amplitude into transverse and longitudinal parts expressing it as $E_m = A_m(z)\psi_m(r,\phi)$. The time averaged intensity will be related to this amplitude by $I_m = \frac{1}{2}\epsilon_0 n_0 c |E_m|^2$. The power is obtained by integrating over the fiber cross section

$$P_m = \int\int I_m r \, dr \, d\phi = \tfrac{1}{2}\epsilon_0 n_0 c |A_m|^2 \int\int |\psi_m|^2 r \, dr \, d\phi$$
$$\equiv N_m^2 |A_m|^2 \ , \tag{8}$$

where

$$N_m^2 = \tfrac{1}{2}\epsilon_0 n_0 c \int\int |\psi_m|^2 r\, dr\, d\phi \ . \tag{9}$$

Define the new longitudinal amplitude as $F_m(z) = N_m A_m(z)$ so that the power becomes $P_m = |F_m|^2$. The electric field can now be expressed as

$$E = \tfrac{1}{2}\sum_{m=1}^{6}\left[\frac{F_m(z)}{N_m}\psi_m(r,\phi)\exp[i(\beta_m z - \omega_m t)] + \text{c.c.}\right] . \tag{10}$$

Now we can separate the wave equation into equations for the six independent frequency components.

As an example of how this is done, consider the ω_1 frequency component of the field. The left-hand side of the nonlinear wave equation contains the linear terms. The simplification of this part proceeds in two stages. First, the axial part of the Laplacian results in the following expression:

$$\frac{\partial^2 E_1}{\partial z^2} = \frac{\psi_1(r,\phi)}{N_1}\exp[i(\beta_1 z - \omega_1 t)] \times\left[\frac{\partial^2 F_1(z)}{\partial z^2} + 2i\beta_1\frac{\partial F_1(z)}{\partial z} - \beta_1^2 F_1(z)\right] . \tag{11}$$

In the slowly varying envelope approximation, the second derivative term will be much smaller than the other terms, and can be neglected. Note that the time derivatives of the field can be replaced by the quantity $-i\omega t$ since we are neglecting any time dependence of the amplitudes by making the quasi-cw approximation. Finally, the left-hand side of Eq. (6) (for the ω_1 frequency component of the field) becomes

$$\nabla^2 E - \frac{n_0^2}{c^2}\frac{\partial^2 E}{\partial t^2} \approx \frac{1}{2}\left[2i\beta_1\frac{\psi_1}{N_1}\frac{\partial F_1}{\partial z} + \frac{F_1}{N_1}[\nabla_T^2\psi_1 + (k_1^2 - \beta_1^2)\psi_1]\right] \times\exp[i(\beta_1 z - \omega_1 t)] . \tag{12}$$

Under the assumption that the transverse modes remain essentially unperturbed by the nonlinearity, the quantity in square brackets in large parentheses is approximately zero, greatly simplifying the left-hand side.[1,4]

Now we must consider the nonlinear part of the wave equation (6). We are interested in determining the components of E^3 that oscillate at the frequency ω_1. There will be three types of terms: terms due to SPM, terms due to XPM, and terms due to FWM.[4] E^3 can be expressed in terms of the triple sum

$$E^3 = \tfrac{1}{8}\sum_{k,m,n} E_k E_m E_n \exp[i(\theta_k + \theta_m + \theta_n)] , \tag{13}$$

where $\theta_k = \beta_k z - \omega_k t$ and $k,m,n = 1,2,3,4,5,6$ and $1^*,2^*,3^*,4^*,5^*,6^*$. The raised asterisk indicates that the complex conjugate is to be taken. The SPM terms occur for combinations like $|E_j|^2 E_j$ which corresponds to index combinations jj^*j of which there are three unique permutations. The XPM terms occur for combinations like $|E_j|^2 E_i$, with $j \neq i$, which correspond to the index combinations jj^*i, of which there are six unique permutations. Finally, there are the FWM terms. These are most easily obtained by considering the generation of the four FWM sidebands from the two pump frequencies as seven FWM processes: the four partially degenerate processes that generate ω_3, ω_4, ω_5, and ω_6 and three nondegenerate processes given by $\omega_1+\omega_2=\omega_3+\omega_4$, $\omega_1+\omega_2=\omega_5+\omega_6$, and $\omega_3+\omega_4=\omega_5+\omega_6$. These latter are obtained from sums of the partially degenerate processes for ω_3, ω_4, ω_5, and ω_6. So the terms containing combinations of frequencies resulting in the frequency ω_1 and their corresponding amplitude products are $E_3E_4E_2^*$ (for $\omega_3+\omega_4-\omega_2$), $E_5E_6E_2^*$ (for $\omega_5+\omega_6-\omega_2$), $E_2E_3E_1^*$ (for $\omega_2+\omega_3-\omega_1$), $E_2^2E_4^*$ (for $2\omega_2-\omega_4$), and $E_3^2E_5^*$ (for $2\omega_3-\omega_5$). The combinations with three different amplitudes have six permutations, and the combinations with only two different amplitudes have three permutations. The necessary terms are generated and the term counting is completed so that we can write down the right-hand side of Eq. (6) remembering to replace the time derivatives by the quantity $-i\omega_1$.

$$\frac{\chi^{(3)}}{c^2}\frac{\partial^2 E^3}{\partial t^2} = -\frac{3\chi^{(3)}\omega_1^2}{8c^2}\left[\left(|E_1|^2 + 2\sum_{j\,(\neq 1)}|E_j|^2\right)E_1 + 2E_2E_3E_1^*\exp(i\phi_{2,3,-1,-1}) + 2E_3E_4E_2^*\exp(i\phi_{3,4,-2,-1}) + 2E_5E_6E_2^*\exp(i\phi_{5,6,-2,-1}) + E_2^2E_4^*\exp(i\phi_{2,2,-4,-1}) + E_3^2E_5^*\exp(i\phi_{3,3,-5,-1})\right]\exp[i(\beta_1 z - \omega_1 t)] , \tag{14}$$

where $\phi_{i,j,-k,-m} = (\beta_i + \beta_j - \beta_k - \beta_m)z$. Now the field amplitudes can be expressed in terms of the separated amplitudes, $E_m = \psi_m(r)F_m(z)/N_m$, and the right-hand side and left-hand side equated. Since we have assumed single-mode propagation, all the ψ_i and N_i are the same. Cancelling the common factors, one obtains the propagation equation for the ω_1 component to be

$$i\beta_1\frac{\partial F_1}{\partial z}=-\frac{3\chi^{(3)}\omega_1^2|\psi_1|^2}{8c^2N_1^2}\left[\left[|F_1|^2+2\sum_{j\,(\neq 1)}|F_j|^2\right]F_1+2F_2F_3F_1^*\exp(i\phi_{2,3,-1,-1})\right.$$
$$+2F_3F_4F_2^*\exp(i\phi_{3,4,-2,-1})+2F_5F_6F_2^*\exp(i\phi_{5,6,-2,-1})$$
$$\left.+F_2^2F_4^*\exp(i\phi_{2,2,-4,-1})+F_3^2F_5^*\exp(i\phi_{3,3,-5,-1})\right]. \tag{15}$$

Let us eliminate the transverse coordinates by multiplying both sides by $|\psi_1|^2$ and integrating over r and ϕ. This results, with some simplifications, in the propagation equation

$$\frac{dF_1}{dz}=\frac{i\omega_1 n_2^I}{cA_{\text{eff}}}\left[\left[|F_1|^2+2\sum_{j\,(\neq 1)}|F_j|^2\right]F_1+2F_2F_3F_1^*\exp(i\phi_{2,3,-1,-1})+2F_3F_4F_2^*\exp(i\phi_{3,4,-2,-1})\right.$$
$$\left.+2F_5F_6F_2^*\exp(i\phi_{5,6,-2,-1})+F_2^2F_4^*\exp(i\phi_{2,2,-4,-1})+F_3^2F_5^*\exp(i\phi_{3,3,-5,-1})\right], \tag{16}$$

where n_2^I is the intensity-dependent refractive index and A_{eff} is the effective core area. These quantities are given by[1,4,13]

$$n_2^I\equiv 3\chi^{(3)}/(4\epsilon_0 c n_0^2)$$

and

$$1/A_{\text{eff}}=\int\int|\psi_1|^4 r\,dr\,d\phi\Big/\left[\int\int|\psi_1|^2 r\,dr\,d\phi\right]^2.$$

The procedure for obtaining the propagation equations for the other frequency components is completely analogous. Before writing these down there are some definitions and simplifications to be made. First, let us define the nonlinearity coefficient γ by $\gamma\equiv\bar{\omega}n_2^I/(cA_{\text{eff}})$, where $\bar{\omega}$ is the average value of the frequency assuming small frequency differences between the FWM components. Also, define normalized amplitudes by letting $F_m=(P_1)^{1/2}U_m$ where P_1 is the input pump power of the pulse at ω_1. Finally, for numerical computations, the linear wave-vector mismatches must be estimated. These are the differences $\Delta\beta_{i,j,-k,-m}=\beta_i+\beta_j-\beta_k-\beta_m$. These can be estimated by assuming that the material contribution to the mismatch is the dominant part and the waveguiding part can be ignored. The wave vector $\beta(\omega)$ can then be expanded about a chosen frequency, ω_1 say, and orders only up to quadratic in the frequency difference kept:

$$\beta(\omega)=\beta^{(0)}+(\omega-\omega_1)\beta^{(1)}+\tfrac{1}{2}(\omega-\omega_1)^2\beta^{(2)}+O((\omega-\omega_1)^3), \tag{17}$$

where $\beta^{(n)}=(d^n\beta/d\omega^n)$ evaluated at $\omega=\omega_1$.[4] There are seven such wave-vector mismatches to be evaluated, one corresponding to each FWM process. The values for these mismatches in terms of the pump detuning $\Omega_{12}=|\omega_1-\omega_2|$ and the second-order dispersion coefficient $\beta^{(2)}$ are given by

$$\Delta\beta_{1,2,-3,-4}=-2\Omega_{12}^2\beta^{(2)}\equiv-2\Delta\kappa, \tag{18a}$$
$$\Delta\beta_{1,2,-5,-6}=-6\Delta\kappa, \tag{18b}$$
$$\Delta\beta_{3,4,-5,-6}=-4\Delta\kappa, \tag{18c}$$
$$\Delta\beta_{1,1,-2,-3}=-\Delta\kappa, \tag{18d}$$
$$\Delta\beta_{2,2,-1,-4}=-\Delta\kappa, \tag{18e}$$
$$\Delta\beta_{3,3,-1,-5}=-\Delta\kappa, \tag{18f}$$

and

$$\Delta\beta_{4,4,-2,-6}=-\Delta\kappa. \tag{18g}$$

Now the complete set of equations for the normalized field amplitudes for the six frequencies can be written down:

$$\frac{dU_1}{dz}=i\gamma P_1\left[\left[|U_1|^2+2\sum_{j\,(\neq 1)}|U_j|^2\right]U_1\right.$$
$$+2U_3U_2U_1^*e^{i\Delta\kappa z}+2U_3U_4U_2^*e^{2i\Delta\kappa z}$$
$$+2U_5U_6U_2^*e^{6i\Delta\kappa z}+U_2^2U_4^*e^{-i\Delta\kappa z}$$
$$\left.+U_3^2U_5^*e^{-i\Delta\kappa z}\right], \tag{19}$$

$$\frac{dU_2}{dz}=i\gamma P_1\left[\left[|U_2|^2+2\sum_{j\,(\neq 2)}|U_j|^2\right]U_2\right.$$
$$+2U_4U_1U_2^*e^{i\Delta\kappa z}+2U_3U_4U_1^*e^{2i\Delta\kappa z}$$
$$+2U_5U_6U_1^*e^{6i\Delta\kappa z}+U_1^2U_3^*e^{-i\Delta\kappa z}$$
$$\left.+U_4^2U_6^*e^{-i\Delta\kappa z}\right], \tag{20}$$

$$\frac{dU_3}{dz}=i\gamma P_1\left[\left[|U_3|^2+2\sum_{j\,(\neq 3)}|U_j|^2\right]U_3\right.$$
$$+2U_1U_2U_4^*e^{-2i\Delta\kappa z}+2U_5U_1U_3^*e^{i\Delta\kappa z}$$
$$\left.+2U_5U_6U_4^*e^{4i\Delta\kappa z}+U_1^2U_2^*e^{-i\Delta\kappa z}\right], \tag{21}$$

$$\frac{dU_4}{dz}=i\gamma P_1\left[\left(|U_4|^2+2\sum_{j\,(\neq 4)}|U_j|^2\right)U_4 +2U_6U_2U_4^*e^{i\Delta\kappa z}+2U_1U_2U_3^*e^{-2i\Delta\kappa z} +2U_5U_6U_3^*e^{4i\Delta\kappa z}+U_2^2U_1^*e^{-i\Delta\kappa z}\right], \quad (22)$$

$$\frac{dU_5}{dz}=i\gamma P_1\left[\left(|U_5|^2+2\sum_{j\,(\neq 5)}|U_j|^2\right)U_5 +2U_1U_2U_6^*e^{-6i\Delta\kappa z}+2U_3U_4U_6^*e^{-4i\Delta\kappa z} +U_3^2U_1^*e^{-i\Delta\kappa z}\right], \quad (23)$$

$$\frac{dU_6}{dz}=i\gamma P_1\left[\left(|U_6|^2+2\sum_{j\,(\neq 6)}|U_j|^2\right)U_6 +2U_1U_2U_5^*e^{-6i\Delta\kappa z}+2U_3U_4U_5^*e^{-4i\Delta\kappa z} +U_4^2U_2^*e^{-i\Delta\kappa z}\right]. \quad (24)$$

Before proceeding to the numerical solution of these equations, let us briefly consider the determination of conserved quantities from the equations for the power, $|U_j|^2$, in each of the six waves. Such quantities would provide a useful check of the numerical solutions. One can obtain the equations for the wave powers from the above amplitude equations by the simple prescription

$$\frac{d|U_j|^2}{dz}=U_j^*\frac{dU_j}{dz}+U_j\frac{dU_j^*}{dz}\ . \quad (25)$$

This results in six power equations involving only the FWM terms, since the SPM and XPM terms cancel out. There are seven types of terms (and their complex conjugates) representing the seven FWM processes. If we let the scaled powers of the waves be $\rho_m=|U_m|^2$ then for the conserved quantities we require that

$$\sum_m \alpha_m\frac{d\rho_m}{dz}=0\ . \quad (26)$$

An obvious choice of conserved quantity for this lossless system of equations is the total power $P_{\rm tot}=\sum_m\rho_m$. The condition for a conserved quantity results in seven equations in six unknowns, the α_m's, due to the linear independence of the seven different FWM terms. However, a row reduction type strategy shows that only four of these equations are independent so that four of the α_m's are determined in terms of two arbitrarily chosen α_m's. Thus one finds that there are two independent constants of the motion from which all others can be generated. Choosing the total power as one and α_1 and α_2 as the arbitrary coefficients one finds the other conserved quantity to be

$$C=(\rho_1-\rho_2)+3(\rho_3-\rho_4)+5(\rho_5-\rho_6)\ . \quad (27)$$

These two conserved quantities were used in our numerical calculations as a check of the integration. The system of Eqs. (19)–(24) were integrated numerically by Gear's method, since they are stiff in character.

III. NUMERICAL INTEGRATION OF PROPAGATION EQUATIONS

The numerical solutions of these coupled, nonlinear, ordinary differential equations display some very interesting dynamical behavior, depending on the choice of parameter values and initial powers for the six frequency components. Before discussing this, however, it is important to know what parameters must be determined to perform the numerical integration. The key parameters are the nonlinearity coefficient γ, the second-order dispersion coefficient $\beta^{(2)}$, and the pump detuning Ω_{12}. The nonlinearity coefficient contains, among other known parameters, the Kerr coefficient for the intensity-dependent refractive index and the effective mode area. The Kerr coefficient was chosen to be a value commensurate with silica fibers. The effective mode area is the more difficult parameter to estimate. The estimate of this parameter was based on calculating the $1/e$ width of the fundamental mode of a step index fiber for the appropriate v number (≈ 2 for a single-mode fiber operating at around 630 nm). The value of $A_{\rm eff}$ could then be calculated based upon this number.[4] The dispersion coefficient was chosen in such a way as to fall within a range reasonable for the optical fiber in the appropriate part of the spectrum (≈ 630 nm) and that would best fit the experimental data. The pump detuning was varied for the numerical studies; it has a known value in the experiments. Finally, the initial conditions, input pump power, and the normalized initial amplitudes for the six frequency components, were chosen based upon experimentally determined values and varied for the purpose of numerical studies. As will be seen presently, the character of the solutions to the coupled wave equations depends strongly on the choice of parameters and initial conditions. All of the numerical studies of this paper will involve a choice of initial conditions for the scaled intensities; for instance, we have mostly used the initial conditions $\rho_1=\rho_2=1$ and $\rho_3=\rho_4=\rho_5=\rho_6=0$. The actual input pump power P_1 and the pump detuning Ω_{12} will be varied in the numerical calculations.

In general, for large detunings and small input powers the numerical solutions show a periodic exchange of small amounts of energy between the pump and first-order sidebands (the second-order sidebands have virtually no energy for these conditions) as a function of propagation distance along the fiber. As the pump power is increased systematically, the behavior remains periodic for the lower P_1 values, but there is a greater exchange of energy between the pump and FWM components. The oscillations also develop more spatial structure. Eventually the behavior becomes chaotic and the Fourier spectrum of power fluctuations becomes very broad, lacking the distinct peaks of the periodic cases. Figures 1(a)–1(c) are a set of trajectories (power versus distance) for one of the pump waves while Figs. 1(d)–1(f) are the associated power

spectra. A quantitative measure of the periodic or chaotic character of the solutions can be obtained by looking at the differences in the trajectories of two numerical solutions with very slightly different initial conditions. Following the treatment of Alekseev *et al.*[10] we define such a measure of trajectory separation to be

$$\Delta(z)=\ln[\delta(z)]=\ln\left[\sum_{m=1}^{6}|U_m(z)-U'_m(z)|^2\right]^{1/2}, \tag{28}$$

where the prime denotes a trajectory with slightly different initial conditions from those of the unprimed trajectory.[10] The trajectory separation was computed for two cases. In the first case the initial conditions were taken to be those for Fig. 1(a) ($\rho_1=\rho_2=1$ and $\rho_3=\rho_4=\rho_5=\rho_6=0$) for the unprimed *periodic* trajectory while for the primed trajectory, ρ_3 was given an initial value of 10^{-6}, all other initial conditions being kept the same. In the second case, the initial conditions were taken to be those of Fig. 1(c) for the unprimed chaotic trajectory, while ρ_3 was given an initial value of 10^{-6} for the primed trajectory. Figures 2(a) and 2(b) show the trajectory separation $\Delta(z)$ plotted for these two cases. Figure 2(a) displays a slow growth of the trajectory separation compared to Fig. 2(b), where the trajectory separation shows a sharp linear increase indicating exponential separation, since this is a logarithmic plot. In Fig. 3(a) we show that the growth of the trajectory separation in the periodic case is approximated quite well by a quadratic. It is clear from Fig. 3(b) that the trajectory separation grows exponentially in the chaotic case. Since this is a bounded, conservative system, the exponential separation of the chaotic case obviously cannot continue indefinitely.

It is also of interest to look at the connection of the dominant frequency in the power spectrum as a function of the pump detuning Ω_{12}. One expects a definite func-

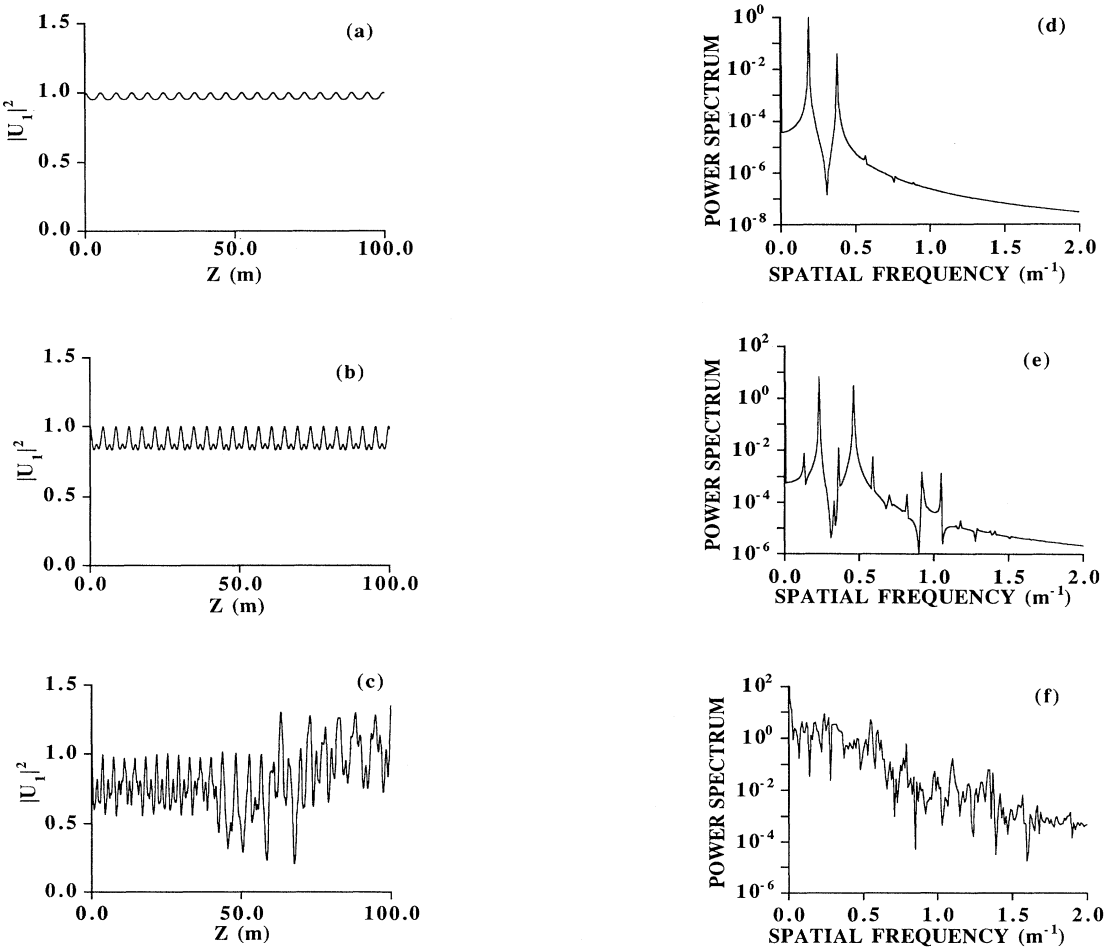

FIG. 1. Transition from simple periodic to chaotic propagation of the intensity of the ω_1 component of the field with increasing input pump power P_1. Frames (a)–(c) show the normalized power in the ω_1 component as a function of propagation distance, and frames (d)–(f) show the corresponding power spectra. The pump-power levels going from simple periodic, to period doubled, to chaotic are $P_1=10$, 30, and 70 W. The parameter values are $\Omega_{12}=20$ cm^{-1}, $\gamma=1.76\times10^{-2}$ m^{-1}W^{-1}, $\beta^{(2)}=70$ ps^2/km, and the fiber length $L=100$ m. The initial conditions for the normalized powers are $\rho_1=\rho_2=1$ for the pump waves and $\rho_3=\rho_4=\rho_5=\rho_6=0$ for the FWM sidebands.

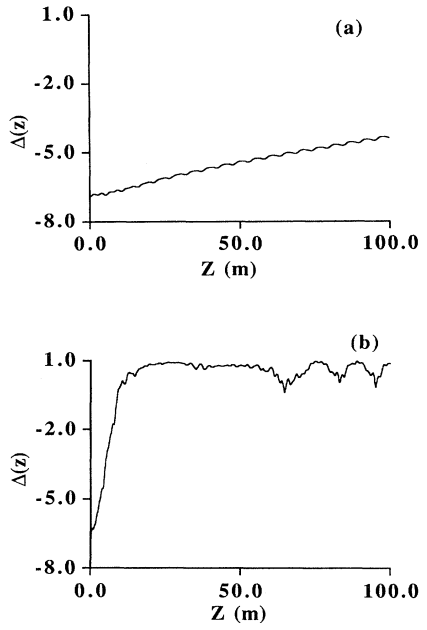

FIG. 2. Dimensionless logarithmic trajectory separation $\Delta(z)$ as a function of propagation distance z. (a) $\Delta(z)$ for two periodic trajectories. The initial conditions for the two trajectories are identical to those for Fig. 1(a), except that ρ_3 is given the initial value 10^{-6} for the primed trajectory. (b) $\Delta(z)$ for two chaotic trajectories. The initial conditions correspond to those for Fig. 1(c), except that ρ_3 is given the initial value 10^{-6} for the primed trajectory.

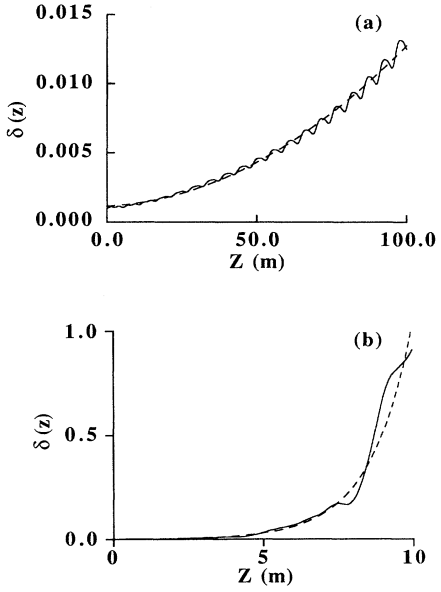

FIG. 3. Plots of the dimensionless linear trajectory separation $\delta(z)$ as a function of propagation distance z. (a) $\delta(z)$ for the two periodic trajectories. The dashed curve is a quadratic polynomial fit to the numerically computed separation. (b) $\delta(z)$ for the two chaotic trajectories. The dashed curve is an exponential fit to the numerically computed separation. Note the difference in vertical scales between the two cases.

tional relationship since the detuning determines the mismatch which appears in the oscillating exponentials of the FWM terms. The fact that for each frequency several such exponentials at different spatial frequencies contribute makes it difficult to anticipate the outcome. The results of such a study are, however, quite simple: There is a quadratic relationship between the dominant spectral component and the pump detuning. Figure 4 shows this relationship for a relatively broad range of detunings.

It is instructive to compare the initial growth of the first-order sidebands for this set of multiple FWM processes with that of the single nondegenerate process $\omega_1+\omega_2=\omega_3+\omega_4$. For the single nondegenerate process the initial growth (neglecting pump depletion), for symmetric initial conditions, can be shown to be given by the analytic expression

$$P_{3,4}=a_0^2\left[1+\left[1+\frac{(\Delta\kappa+3\gamma P_1)^2}{g^2}\right]\sinh^2(gz)\right], \quad (29)$$

where g is the gain defined by $g=[(2\gamma P_1)^2-(\Delta\kappa+\gamma P_1)^2]^{1/2}$ and a_0 is the normalized initial amplitude of the first-order FWM peaks.[1,4] Figure 5 shows the comparison between the two cases for the growth of the first-order FWM sidebands. Note that the hyperbolic sine growth of the analytic solution Eq. (29) is very slow compared with the results from numerical integration of Eqs. (19)–(24). This is to be expected since in the case of multiple FWM processes there are several contributions to the growth of the first-order peaks. More significantly, one of these contributions involves the cube of the pump fields, as opposed to growth proportional to the square of the pump fields and the (small) first-order peak for the nondegenerate case.

IV. EXPERIMENTAL RESULTS

The propagation equations (19)–(24) may be tested directly by comparison of the results of numerical in-

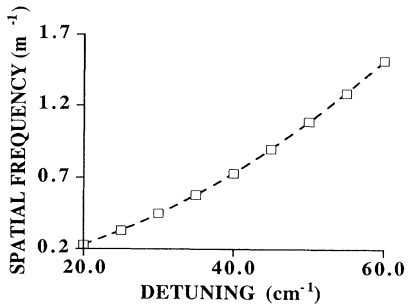

FIG. 4. Dependence on the pump detuning Ω_{12} of the dominant spatial frequency in the power spectrum of one pump wave propagation trajectory. The solid squares show the dominant spatial frequency in the power spectra obtained for different detunings. The dashed line shows a quadratic polynomial fit to the data. The parameters γ, β, and L and the initial conditions for the normalized powers are identical to those of Fig. 1, and the input pump power is $P_1=30$ W for all the points.

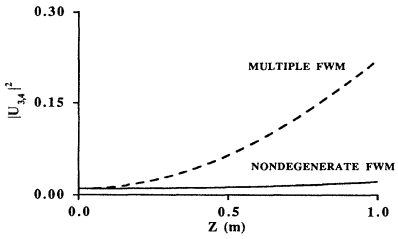

FIG. 5. Comparison of the initial growth of the analytic solution [Eq. (29)], that neglects pump depletion, for the single nondegenerate FWM process $\omega_1+\omega_2=\omega_3+\omega_4$, with the numerical solution for multiple FWM processes. The parameters γ and β are the same as for earlier figures. The initial normalized powers were $\rho_1=\rho_2=1$ and $\rho_3=\rho_4=0.01$. The pump detuning was $\Omega_{12}=2$ cm^{-1} and the input pump power was $P_1=20$ W. The numerical results are virtually identical whether the first-order sidebands only are included or the second-order sidebands are included as well.

tegration with experimental measurements of the sideband peaks generated when two pump waves with a given detuning are launched into the fiber. Figure 6 is a schematic representation of the experimental apparatus. The pulses (5 ns long) from two tunable, pulsed, dye lasers, pumped by a frequency-doubled Nd:YAG laser (YAG denotes yttrium aluminum garnet), are linearly polarized and launched along a principal axis of a 1.5-m length of single-mode polarization maintaining fiber with a core diameter of 4 μm. The output of the fiber is then directed into a spectrometer, and the spectrum is recorded by a charge-coupled device (CCD) camera. The spectral image is digitized and stored by a frame grabber in a microcomputer. The pump detunings can be determined to an accuracy of $\sim$0.05 nm with the spectrometer system. It is possible to obtain single shot spectra as well as spectra averaged over a large number of laser pulses. Figure 7(a) shows a spectrum of the light at the fiber output averaged over 100 pulses. The two pump pulses are adjusted to be of approximately equal intensity. Also seen are the two first-order FWM sidebands. The input pump waves are equal (17.6 W) in intensity. When the power of the pump waves is increased to 163 W, several orders of FWM sidebands are generated in the fiber. This is illustrated in Fig. 7(b). In making comparisons with theory we have restricted the pump wave power levels to below 100 W, when only the first-order sidebands are appreciable in strength. Even though the second-order sidebands are very small compared to the pump waves and first-order sidebands, they play a critical role for obtaining good agreement between experiment and theory at the higher pump-power levels.

There were two types of measurements made that provide stringent tests of the theory for lengths of fiber on the order of a meter and peak input pump powers of <100 W. The first set of measurements determined the dependence of the output power of the first-order sidebands on the input pump power for a given pump detuning. For these experiments the pump detuning Ω_{12} was set to some previously chosen value and the input pump power varied over a range of 10–100 W. The output powers (as a fraction of the pump) of the first-order sidebands were then determined from the averaged spectra. Figure 8 shows the experimental data for two pump detunings (19.5 and 30.5 cm^{-1}) and the corresponding theoretical match (solid curves). The agreement between experiment and theory is quite good over the entire range of the input pump powers. The same values of the nonlinearity coefficient γ and the second-order dispersion coefficient $\beta^{(2)}$ were used for both calculations.

A point of interest here is the question of why six frequencies, instead of four, were included in the theoretical model since our experiments are soley concerned with the

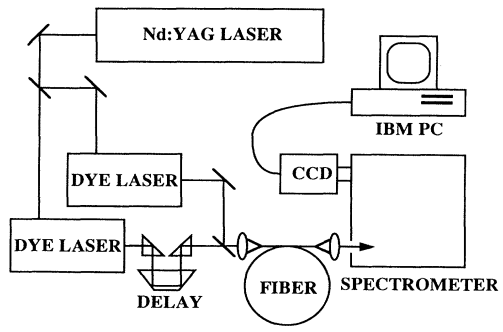

FIG. 6. Experimental apparatus for the study of FWM in single-mode optical fiber.

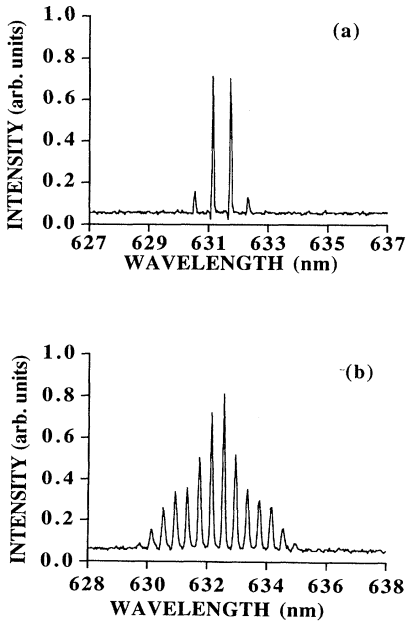

FIG. 7. Typical FWM spectra for low and high input pump powers. (a) $P_1=P_2=17.6$ W, detuning between pump waves of 14.8 cm^{-1}. Only the first-order sidebands are prominent. (b) $P_1=P_2=163$ W, detuning between the pump waves of 10 cm^{-1}. Sidebands up to the sixth order are clearly visible.

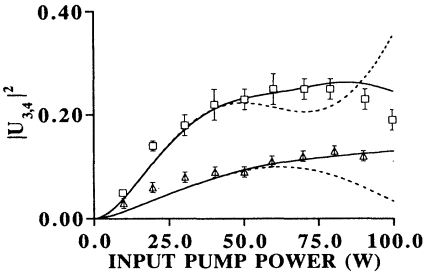

FIG. 8. Plots showing the dependence of the normalized first-order sideband power (as a fraction of the input pump power P_1) on the input pump power. The open squares are for a pump detuning of 19.5 cm^{-1} and the open triangles for a pump detuning of 30.5 cm^{-1}. The solid curves are computed by numerical integration of Eqs. (19)–(24). The dashed curves show the behavior when only the first-order sidebands are included in the numerical solution. The values of the parameters γ and β and the initial normalized powers for the six waves are the same as in Fig. 1. The fiber length $L=1.5$ m. The parameter values and initial conditions are the same for the solid and dashed curves.

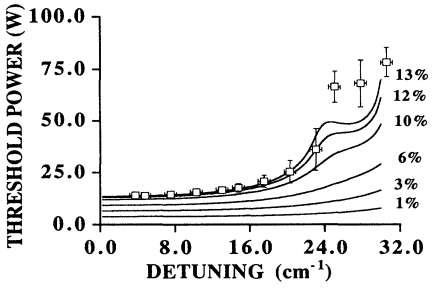

FIG. 9. Plots showing theoretical curves of the input pump power necessary for the first-order sideband power to reach preset percentages of the pump, as a function of the pump detuning Ω_{12}. The open squares are experimentally determined threshold pump powers for the sidebands to reach 13% of the pump strength at the end of the 1.5-m fiber. The error bars represent uncertainties in the determination of the pump thresholds and detunings. The parameter values and initial powers for the calculations were the same as for Fig. 8.

first-order sidebands. When the first-order sidebands become strong enough it is possible for them to mix with the pump frequencies to generate two additional sidebands. In fact, one can easily experimentally generate spectra with as many as a dozen peaks for sufficiently high input power. It was conjectured that for higher input pump powers in our experiments (in the range of 50–100 W) the second-order peaks might play a significant role in the FWM processes. This was subsequently confirmed by the fact that the experimental data could not be matched with realistic choices of parameters by taking into account only the first-order sidebands. The dashed curves in Fig. 8 illustrate the significant influence of the second-order sidebands on the behavior of the first-order sideband peaks. All the parameter values and initial conditions used for computations with only four waves are the same as in the model with six waves.

The second set of measurements used as a test of the theory determined the input pump power P_1 necessary to generate first-order sidebands with a preset threshold percentage of the input pump power as a function of the pump detuning Ω_{12}. For these experiments the pump detuning was varied over a range of $\sim 3-30$ cm^{-1}. For each detuning the pump power was adjusted so that the average first-order sideband power was approximately at the preset threshold. Figure 9 shows the experimental data for a threshold of 13%. Also shown is the theoretical fit and other calculated curves for different threshold values. The data fit the calculations quite well for the smaller detunings. For the largest detunings experiment and theory do not agree as well as in the case of small detunings, although there is qualitative agreement in the shape of the curves. The disagreement for large detunings may be due to the influence of Raman scattering since for these the input pump power is significantly larger than for the small detunings. Also, spectral broadening due to SPM and XPM, neglected in our quasi-cw treatment, will be of increasing importance for higher pump powers for our ~ 5-ns pulses. For these calculations the same values of γ and $\beta^{(2)}$ were used as for the calculations of Fig. 8.

The series of curves for different choices of threshold show an interesting change in behavior as one goes to progressively higher threshold percentages. All curves

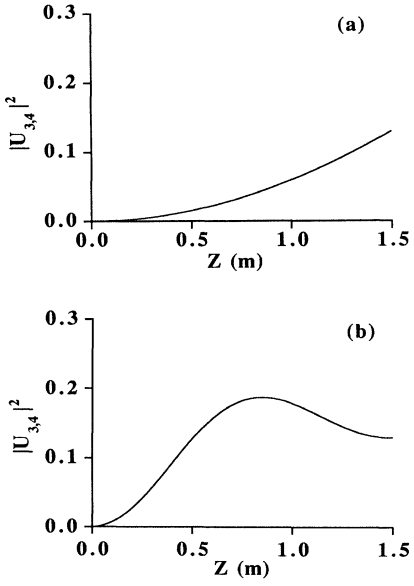

FIG. 10. Plots showing the difference in the growth of the first-order sidebands for two points on the 13% threshold curve of Fig. 9. (a) Input pump power of $P_1=13.9$ W and a pump detuning of $\Omega_{12}=6$ cm^{-1}. (b) Input pump power $P_1=48.5$ W and a detuning of $\Omega_{12}=24$ cm^{-1}.

are quite flat for small detunings and increase more steeply for larger detunings. For larger values of sideband threshold a kink develops at a detuning of $\sim 24\ \mathrm{cm}^{-1}$. For this region of the curve it is observed that the growth of the FWM peaks along the fiber length is no longer monotonic; there is an exchange of energy between pump and FWM peaks. Figures 10(a) and 10(b) show the growth of one of the first-order sidebands for small and large detunings, respectively. In Fig. 10(a) the power trajectory is monotonic, while in Fig. 10(b) it is not. In the latter case, it is more difficult to determine the threshold pump power needed to achieve a certain sideband amplitude, resulting in the larger error bars for this regime of measurements (large detunings and high peak powers) in Fig. 9.

V. CONCLUSION

We have developed a model to describe multiple four-wave mixing processes in an optical fiber. The propagation equations for two pump waves and four sidebands generated by FWM processes are considered in the model. Conserved quantities are determined for this system of equations. From numerical integration of these equations we find that both periodic and chaotic exchange of energy between the pump and FWM sidebands may occur during propagation through the fiber. For practical applications, this implies that the power at the pump frequencies may fluctuate chaotically from pulse to pulse at the output of the fiber for sufficiently high powers and small detuning between the pump waves. We have directly tested predictions obtained from the model equations in experiments on an optical fiber with two tunable pump waves.

ACKNOWLEDGMENTS

It is a pleasure to acknowledge very helpful discussions with Vladimir Yakhnin and Girish Agarwal on the theoretical model presented here, and Bill Gardner of AT&T Bell Laboratories for providing us with the single-mode fiber. We thank Janet Dixon for her help in the initial stages of the experiments and Tom Maier for his patient and generous help with the electronics for the digitized spectrum acquisition system. J.T. and R.R. acknowledge support from the Department of Energy, Office of Basic Energy Sciences, Chemical Sciences Division.

[1]R. H. Stolen and J. E. Bjorkholm, IEEE J. Quantum Electron. **QE-18**, 1062 (1982).
[2]R. K. Jain and K. Stenersen, Appl. Phys. B **35**, 49 (1984).
[3]K. Stenersen and R. K. Jain, Opt. Commun. **51**, 121 (1984).
[4]G. P. Agrawal, *Nonlinear Fiber Optics* (Academic, San Diego, 1989).
[5]Y. Chen and A. W. Snyder, Opt. Lett. **14**, 87 (1989).
[6]Y. Chen, J. Opt. Soc. Am. B **6**, 1986 (1989).
[7]S. Trillo and G. Cappellini (unpublished).
[8]S. Wabnitz, Phys. Rev. Lett. **58**, 1415 (1987).
[9]D. David, D. D. Holm, and M. V. Tratnik, Phys. Rep. **187**, 281 (1990).
[10]K. N. Alekseev, G. P. Berman, A. V. Butenko, A. K. Popov, V. M. Shalaev, and V. Z. Yakhnin, J. Mod. Opt. **37**, 41 (1990).
[11]N. N. Alekseeva, K. N. Alekseev, V. A. Balueva, G. P. Berman, A. K. Popov, and V. Z. Yakhnin (unpublished).
[12]T. Okoshi, *Optical Fibers* (Academic, Orlando, 1982), Chap. 4.
[13]P. N. Butcher and D. Cotter, *The Elements of Nonlinear Optics* (Cambridge University Press, New York, 1990), Appendix 5.